Civil Engineering Dimension, Vol. 24, No. 2, September 2022, 85-92
ISSN 1410-9530 print / ISSN 1979-570X online
DOI: 10.9744/CED.24.2.85-92

Nonlinear Finite Element Analysis of Flexural Laminated Veneer Lumber (LVL) Sengon Slender Beam

Effendi, M.K.[1] and Awaludin, A.[2]*

Abstract: Laminated Veneer Lumber (LVL) is one of the engineered wood products consisting of wood veneers that are glued and pressed together. In this study, the behavior of LVL Sengon slender beam is numerically investigated by means of nonlinear finite element analysis (FEA), where only half of the experimental beam was modeled due to symmetry of the load configuration. The LVL Sengon wood material used Hill failure criterion with isotropic hardening rules, and its mechanical properties in both tension and compression are modelled according to its mechanical properties in tension obtained from the clear specimen test. The contact analysis is defined for each contacting and contacted elements. The FEA results well agreed with the experimental results in term of the load-deflection curve and failure mode of the beam. It is found that the lateral support has no effect on the stiffness of the beam. The beam stiffness and ultimate load increase by the increase of beam height-to-width ratio (*d*/*b*).

Keywords: LVL; slender beam; failure criterion; finite element analysis; lateral support.

Introduction

Housing construction in Indonesia is expected to increasingly continue in the coming years. Houses are generally built using reinforced concrete material. This reinforced concrete material is one of a large share of global emissions [1]. The process of wood processing from raw materials to production or the cradle-to-gate process produces lower CO_2 emissions compared to concrete, steel, or brick constructions [2–5]. Therefore, building structural materials with wood materials should be introduced in Indonesia to overcome these CO_2 emission issue. In addition to having the advantage of low CO_2 emissions, this wood material has disadvantage in some cases in which larger beam or column dimensions are required for heavy building construction. It is very difficult to get large or extra-large size of wood on the market. One way to overcome this problem is to use laminated wood products.

Laminated Veneer Lumber (LVL) is one of the engineered wood products consisting of wood veneers that are glued and pressed together. Sengon (*Paraserianthes falcataria*) wood is very familiar to be used for LVL material because it is easy to cultivate and has a very short planting age of about 5 years [6]. LVL Sengon wood has started to be widely used as building structural elements [7–9]. This LVL can be used for beam construction elements. However, for the use of slender beams which are having a large *d*/*b* ratio are prone to overturning/torsion [10]. This torsion can be overcome with lateral restraints. The study of lateral confinement on the beam at support has been carried out by Awaludin, *et al.* [11] experimentally and numerically using finite element analysis. The nonlinear load-displacement response was obtained from the experimental results, while the finite element analysis produced a linear response only. For laminated beams with a large *d*/*b* ratio loaded without lateral supports, Xiao *et al.* [12] conducted experimental and finite element analysis. Study on the flexural behavior of wooden beams given lateral confinement at the center of the span has been studied numerically by Hu, *et al.* [13] and a numerical study on the behavior of high beams, by modeling geometric imperfections using slips subjected to lateral reinforcement has been studied by Klasson *et al.* [14]. So far, contact analysis was not taken into account in the finite element analysis.

The aim of the present work is to numerically predict the flexural capacity of LVL Sengon slender beam by means nonlinear finite element analysis (FEA). The analysis includes the contact analysis between contacted and contacting body. This study uses a commercial FEA sotware, MSC Marc/Mentat [15]. Experimental specimen [11] is used for the comparison of the FEA present study. To provide researchers and engineers a better understanding of the LVL Sengon slender beam, parametric study about influences of lateral support depth and height-to-width (*d*/*b*) ratio of beam cross-section are also investigated by means of the present FEA model.

[1] Department of Civil Engineering, Faculty of Civil Engineering and Planning, Universitas Islam Indonesia, Yogyakarta, INDONESIA
[2] Department of Civil and Environmental Engineering, Faculty of Engineering, Universitas Gadjah Mada, Yogyakarta, INDONESIA
*Corresponding author; Email: ali.awaludin@ugm.ac.id

Note: Discussion is expected before November, 1st 2022, and will be published in the "Civil Engineering Dimension", volume 25, number 1, March 2023.

Received 1 May 2022; revised 12 June 2022; accepted 22 July 2022.

Research Method

This paper presents a numerical simulation of LVL slender beam by using the three-dimensional finite element model. The non-linear material and non-linear geometry of the beam are analyzed by means of finite element package, MSC Marc/Mentat [15]. A full scale LVL beam made by several layers of thin Sengon wood tested by Awaludin, *et al.* [11] was chosen to validate the numerical model.

Geometry of the LVL Beam

The modeled LVL slender beam specimen is obtained from the available experimental test carried out by Awaludin, *et al.* [11]. The beam was tested until failure under a three-point bending test, as shown in Fig. 1. Laminated Veneer Lumber (LVL) beams is made by 25 layers of Sengon wood veneer with a thickness each approximately 2 mm. The beam is 2500 mm long, and it has dimension of 50 mm wide and 250 mm height. At both ends, the lateral supports are given with C-section steel profile to avoid rotation at supports. The length of the lateral supports is 50 mm, thus the effective span of the beam is 2400 mm.

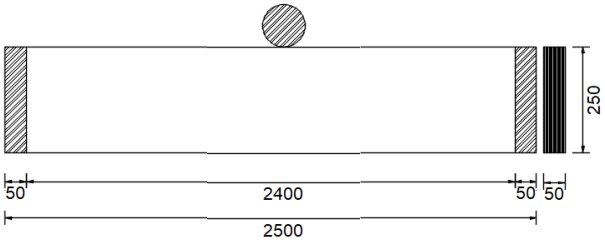

Figure 1. Geometry of the LVL Beam for FEA Study

Finite Element Modeling

In the FEA model created, LVL beam is modeled as three-dimensional element. The LVL Sengon wood layers, the steel loading transfer plate, and the steel support plate are modelled using the 3D solid elements, type 7 in MSC Marc/Mentat [16]. The element has eight nodes and three degrees of freedom at each node, translations in the nodal *x*, *y*, and *z* directions.

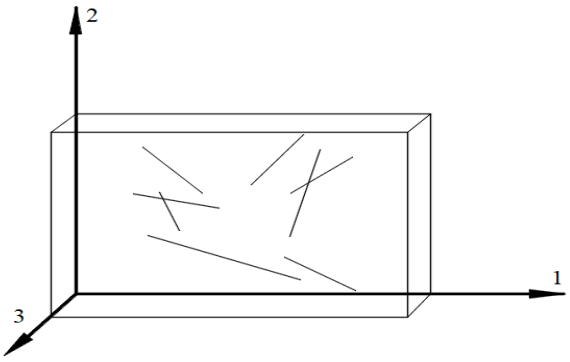

Figure 1. Local Axes of Sengon Wood Element

Table 1. Material Properties of Sengon Wood

Parameter		Tension	
MoE	E_1	7083 MPa	[17]
	E_2	7083 MPa	[17]
	E_3	60.26 MPa	
Poisson's Ratio	υ_{12}	0.225	[18]
	υ_{13}	0.005	[18]
	υ_{23}	0.225	
Tensile Stress	σ_u	46.69 MPa	[17]
Yield Stress	σ_y	46.69 MPa	
Shear Modulus	G_{12}	919.6 MPa	
	G_{13}	919.6 MPa	
	G_{23}	919.6 MPa	

Hill failures and Hill yield criterion with isotropic hardening rules were used for the LVL Sengon material. The Hill yield criterion can be thought of as an extension of the von-Mises yield criterion [19]. The wood mechanical properties in both tension and compression are modelled based on the mechanical properties in tension. Based on this assumption, as seen in Table 1, the tension mechanical properties are used as the material input. Material properties for uniaxial behavior of LVL with anisotropic plasticity model for multi-layer sandwich beam with random stacking sequence is used in the analysis of a notched shear block test specimen and a single-bolt connection [20]. For the present FEA study, the Sengon layers behavior is assumed to be the multi-layer sandwich beam with random stacking sequence. The local direction axes of Sengon wood can be seen in Figure 1. The input of elastic modulus of Sengon layers is assumed to be the same value with respect to local direction 1, and local direction 2, which is 7083 MPa, whereas elastic modulus of 60.26 MPa is assigned in local direction 3. The shear modulus is assumed the same value with respect to local direction 1, 2 and 3, respectively which is 919.6 MPa. The LVL Sengon layers are assumed as elastic perfectly plastic material with respect to both parallel-to-grain and perpendicular-to-grain as can be seen in Figure 2. The tensile strength with respect to X axis is taken as 46.69 MPa while the tensile strength with respect to Y and Z axes is 10% of the X axis stress [21].

The steel support and steel loading transfer plate materials are modeled as the linear-elastic material. For the specimens considered, only half of the experimental beam was modeled due to symmetry. The mesh of the test specimen can be seen in Fig. 3. The mesh for steel support is 25x25x25 mm size and

the number of elements is 4 solid elements. To obtain reasonable results with the experimental results, the LVL Sengon layers mesh is 25x25x2 mm. This mesh size produces a total mesh of 12500 solid elements. This number of solid elements are considered to have given converged results. Because of the computer's capability, the FEA model running time is very long if more than 12500 solid elements are used. The mesh of steel loading solid tube is made by dividing the tube into triangular elements in the near center of the mesh and rectangular elements in others. The loading elements are 84 solid elements.

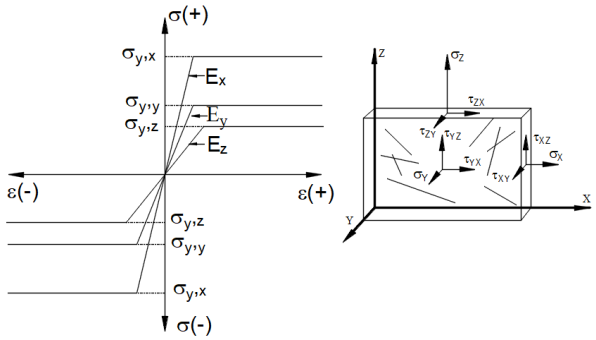

Figure 2. Geometry of the LVL Beam for FEA Study

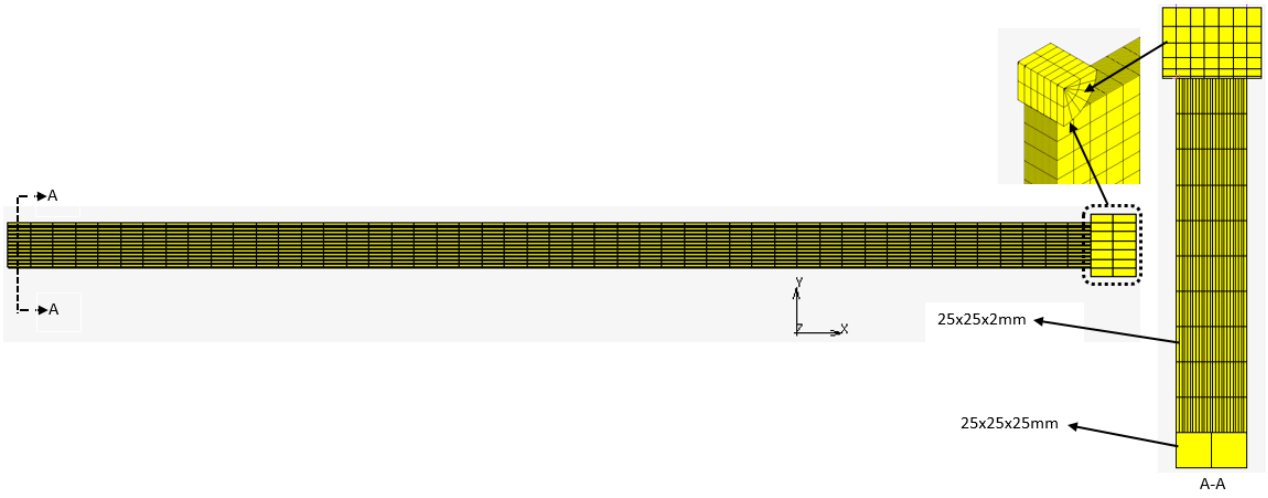

(a) (b)

Figure 3. The mesh of LVL Sengon Beam

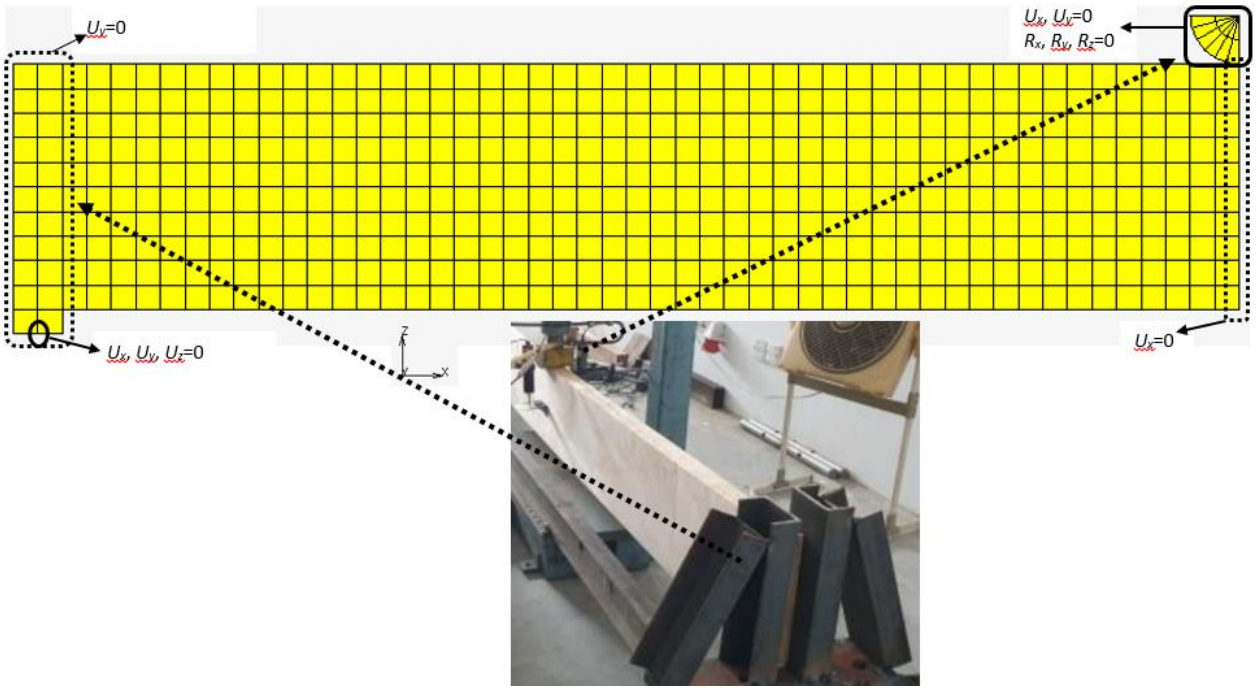

Figure 4. The Load and Support Conditions

The boundary conditions and loading conditions on the FEA LVL beam model were set the same as the beam conditions during the experiment. This condition, if they are not properly defined, will affect the results of the FEA so that it produces a different response from the experiment. To model the half-span beam, all degrees of freedom of node translation in the X direction at the right cross section are restrained, $U_x = 0$. Loading is carried out with displacement control where the load element is given a displacement in the direction of U_z by 40 mm downwards, negative Z direction. In the load element, the translational degrees of freedom, U_x, U_y, and the rotation of R_x, R_y, R_z were set to zero. For the supports, to model the pin support, the degrees of freedom U_x, U_y, U_z were set to zero on the middle nodes on lower nodal element supports. The condition of the beam element above the support where the lateral support is installed, the degrees of freedom U_y were set to zero. Illustrations of load and boundary conditions are shown in Figure 4.

Contact Conditions

From the experiment [11], there was contact between the steel loading transfer plate and the LVL Sengon beam. In addition, there was also contact between the steel supports and the LVL Sengon beam. The contacted and contacting elements are composed of contact body type deformable elements. Contact analysis is the contact type touching. This type allows the contact elements to separate each other. Contact also occurs between the Sengon layers of the LVL Sengon beam. The contact analysis type for the each Sengon layers is glue. The glue type means that the contact element should be treated as one part. The details of the contact pairs can be seen in Fig. 5. By defining the contact table in MSC Marc/Mentat, the contact pairs are defined. The default parameters in the contact table are used in this study.

Hill Failure Indicator

There are some of the widely used theories for analyzing material failures, such as Tsai-Hill, Tsai-Wu, and failure criteria Hoffman, maximum stress and strain maximum [22-25]. The Tsai-Hill failure indicator, σ_o is used in the analysis and may be expressed as Eq. 1:

$$\sigma_o = \sqrt{F_A(\sigma)} = \sqrt{H(\sigma_{11}-\sigma_{22})^2 + F(\sigma_{22}-\sigma_{33})^2 + G(\sigma_{33}-\sigma_{11})^2 + 2N\sigma_{12}^2 + 2L\sigma_{23}^2 + 2M\sigma_{31}^2}$$

$$F = \frac{1}{2}\left(\frac{1}{R_{22}^2}+\frac{1}{R_{33}^2}-\frac{1}{R_{11}^2}\right) \quad L = \frac{3}{2}\left(\frac{1}{R_{23}^2}\right) \quad R_{11} = \frac{\sigma_{11}^y}{\sigma_o} \quad R_{12} = \sqrt{3}\frac{\sigma_{12}^y}{\sigma_o}$$

$$G = \frac{1}{2}\left(\frac{1}{R_{33}^2}+\frac{1}{R_{11}^2}-\frac{1}{R_{22}^2}\right) \quad M = \frac{3}{2}\left(\frac{1}{R_{13}^2}\right) \quad R_{22} = \frac{\sigma_{22}^y}{\sigma_o} \quad R_{23} = \sqrt{3}\frac{\sigma_{23}^y}{\sigma_o}$$

$$H = \frac{1}{2}\left(\frac{1}{R_{11}^2}+\frac{1}{R_{22}^2}-\frac{1}{R_{33}^2}\right) \quad N = \frac{3}{2}\left(\frac{1}{R_{12}^2}\right) \quad R_{33} = \frac{\sigma_{33}^y}{\sigma_o} \quad R_{13} = \sqrt{3}\frac{\sigma_{13}^y}{\sigma_o}$$

Where: $\sigma_{11}^y, \sigma_{22}^y, \sigma_{33}^y, \sigma_{12}^y, \sigma_{23}^y, \sigma_{13}^y$ are the normal and shear in yield condition with respect to the axes, respectively. The Hill failure is deemed to occur when the indicator reaches or exceeds the value of 1. The constants R_{11}, R_{22}, R_{33}, R_{12}, R_{23}, R_{13} represent that ratio of the yield stress in a given direction to the reference (von Mises) yield stress. Hill's criterion does not describe hardening, it only describes the yield criteria. The Hill potential is combined with isotropic hardening models. The Hill model is then used to determine the actual yield stress value in six directions. The von Mises criterion is often used to estimate the yield of very ductile materials, with the same yield strength in tension and in compression [26].

Results and Discussion

Load-Deflection Response

A half of the LVL Sengon beam is modelled in the analysis. The response of the LVL beam under static load at midspan of the beam is represented by the graph of load versus displacement. The load is the summation of the two times vertical reaction forces. The displacement is measured at mid-section of the midspan of the beam. Figure 6 shows the load-displacement curves of the beam by both experiment and FEA study [11] and the present FEA simulation. The experimental load-deflection curve obtained from testing in the laboratory in which the maximum load is 27.88 kN and maximum displacement is 28.59 mm, respectively [11]. In FEA Sengon LVL beam behaves in linear response because the material is assumed to behave elastically and linearly [11]. As shown in the Fig. 6, the present FEA results show tri-linear shaped load-displacement curve. The beam behavior of present FEA study results is linear up to a load level of 10 kN (p_1), after which a small non-linearity was initiated and then continued increasing until about 20 kN (p_2) and the second non-linearity until the load corresponds to 38.59 mm displacement reached about 25.7 kN (p_3). This load (p_3) is almost the same as the load given by the experiment 27.88 kN where the difference is about less than 10%.

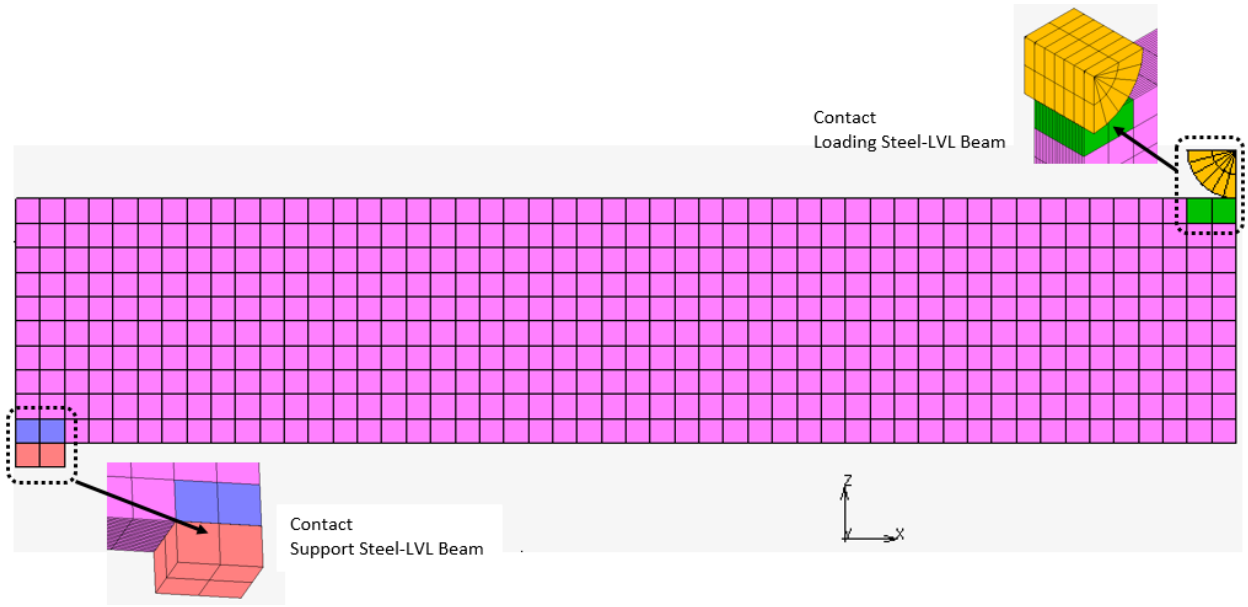

Figure 5. Contact Analysis.

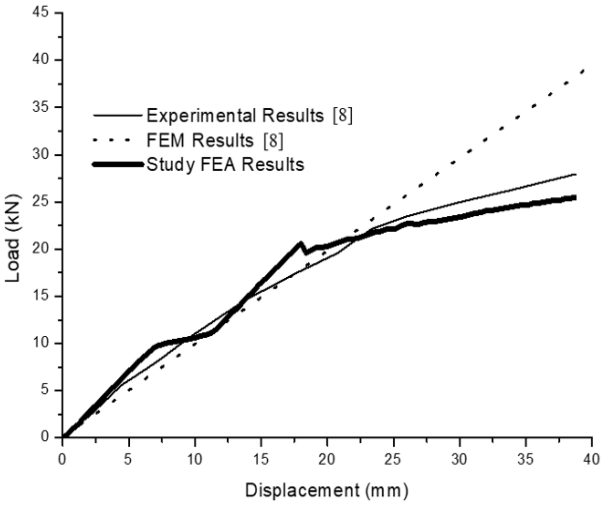

Figure 6. Load–deflection Response

Failure Mode

Figure 7 shows the failure mode of the LVL slender beam obtained from the present FEA. According to the test results as shown in Figure 7(b), it also indicates that the local damage was occurred at the upper side of the beam close to the loading point and at bottom side of the LVL beam. The failure mode of present FEA results shows the same phenomenon as that of experimental results. The Fig. 7(a) display the isometric view and Figure 7(c) shows the side view of the present FEA of the finite element analysis. The lateral deformation was found 12 mm under the steel loading transfer plate as shown in Figure 7(a) when the load reaches ultimate of 25.7 kN. There is no indication of separation between the LVL layers because in the FEA modeling LVL layers are considered as fixed at contact surface.

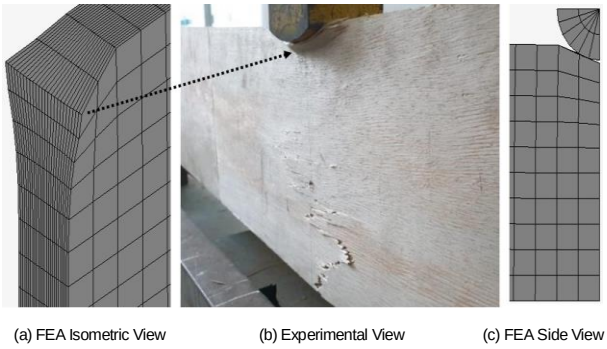

Figure 7. Failure LVL Sengon Beam (a) FEA Isometric View (b) Experimental View (c) FEA Side View

Failure Index

The failure of the LVL beam is evaluated by the Hill failure criteria. The evaluation of Hill failure criteria was carried out by MSC Marc/Mentat software. The software displays the failure index for each layer of the LVL beam. From the Fig. 8, it displays the failure index above 1. The display is set to be above 1 which means the layer/beam is failure. The failure is occurred in the bottom mid-span of the beam and below the loading until the mid-section of the beam. From the Figure 8, the experimental failure also occurs in the bottom mid-span of the beam and at the beam below the loading point. Failure of the finite element analysis is almost the same as that of the experimental result.

Influences of Lateral Support Depth

The possible failure mode of lateral torsional buckling (LTB) is prone to happen in a slender beam. With all the same material parameter as present study, a

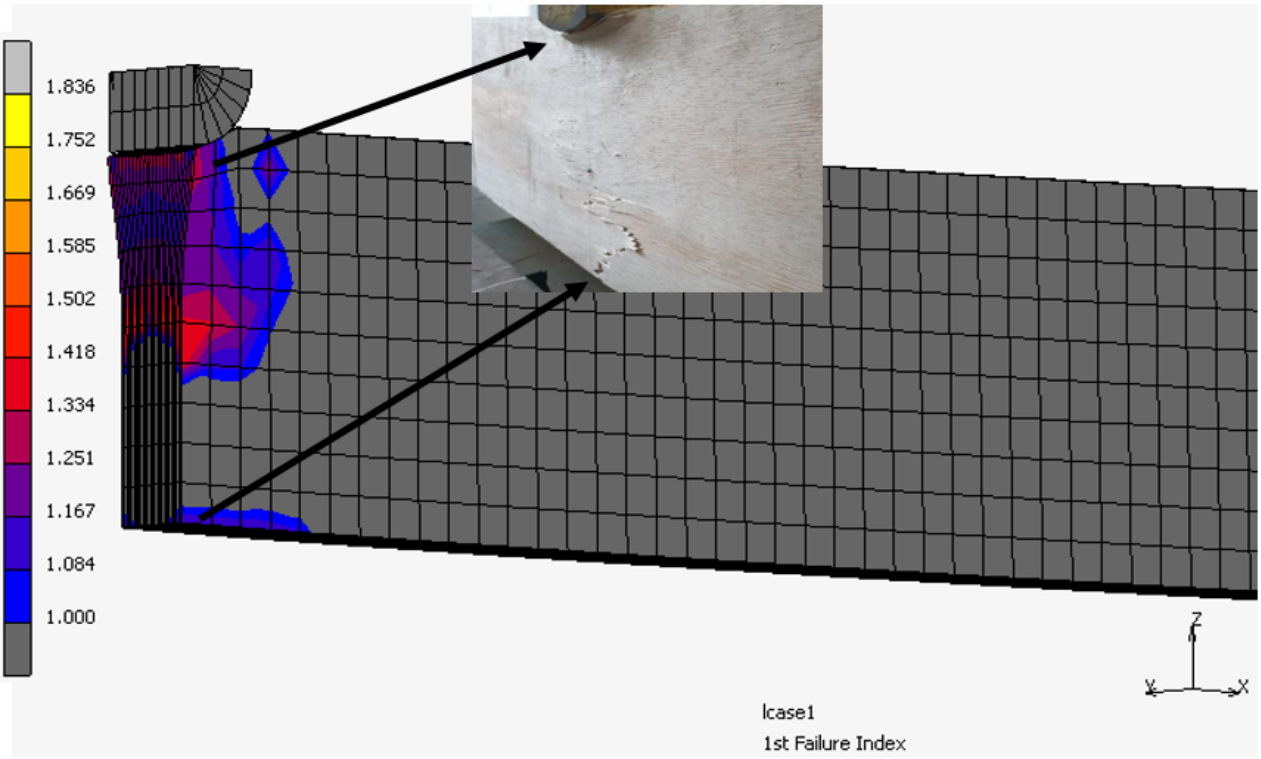

Figure 8. Failure Index

parametric study of the lateral support depth on load-displacement behavior is examined. The parametric study could be performed as the present FEA model has proven its capability produce the numerical results with high degree of agreement with the experimental results. To study the lateral torsional buckling, additional lateral supports are provided to the beam in the plane of the compression of beam 25 mm and 50 mm from top fiber along the beam and at both end supports. The beam will be given a 40 mm displacement loading at mid span of the beam. As seen in Figure 9(a), LVL beam with lateral support at both supports only produces a linear response load of 10 kN, whereas with addition 25 mm and 50 mm lateral supports linear response are 20 kN and 25 kN, respectively. All beams, after generating linear response, experienced short plastic condition followed by an increasing load. Ultimate beam load with lateral support at both supports only, at both supports plus 25 mm from top fiber along the beam, and at both supports plus 50 mm from top fiber along the beam produce loads of 25.7 kN, 27.8 kN and 30.5 kN, respectively. The stiffness of all beams, load per unit deflection, is about 1.4 kN/mm. The lateral support depth has no effect on the stiffness of the beam. The failure mode of the beam in the plane of the compression of beam 25 mm and 50 mm from top fiber along the beam and at both supports can be seen in Figure 9(b).

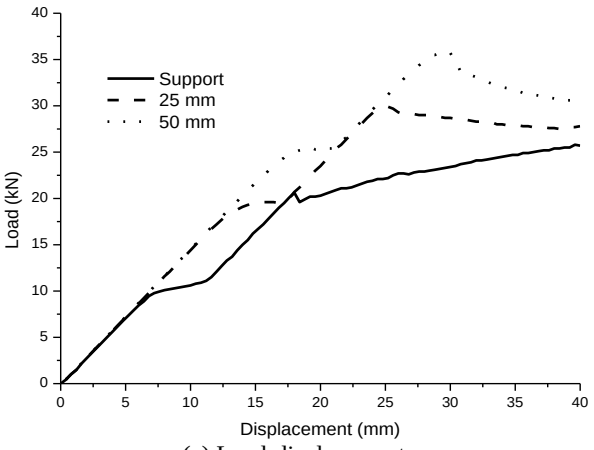

(a) Load-displacement

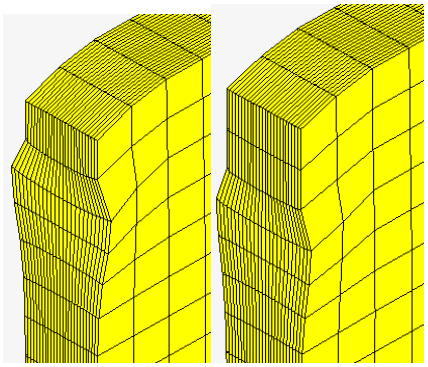

(1) 25 mm (2) 50 mm

(b) Failure Mode

Figure 9. Parametric Study of Lateral Support Depth

Influences of Ratio of Height-to-width (*d*/*b*) of Beam Cross-section

The same procedure is used to study the influence of height-to-width (*d*/*b*) ratio of beam cross-section on the load-displacement behavior of LVL beam. The beam size parameter is 50x100 mm, 50x150 mm, 50x200 mm, and 50x250 mm. The beam is restrained laterally at both end supports and is given displacement control maximum 40 mm. From Fig. 10, the beam size 50x100 mm and 50x150 mm shows the linear response during the analysis, on the other hand, the beam size 50x200 mm and 50x250 mm shows the nonlinear response during the analysis. The load capacity of the higher depth of the beam size is higher than the lower depth of the beam size. The load corresponds to 28.59 mm displacement of the beam size 50x250 mm, 50x200 mm, 50x150 mm, and 50x100 mm, are 3.86 kN, 11.4 kN, 19.8 kN, and 25.7 kN, respectively. The results of this analysis are in good agreement with the study conducted by Oka [27]. The beam size has effect on the beam load capacity. The higher depth of the beam, the higher load capacity of the beam. The stiffness of beam size 50x250 mm, 50x200 mm, 50x150 mm, and 50x100 mm, load per unit deflection, are about 0.09 kN/mm, 0.31 kN/mm, 0.74 kN/mm, and 1.4 kN/mm, respectively. The beam size has effect on the stiffness of the beam, the higher depth of the beam, the higher stiffness of the beam.

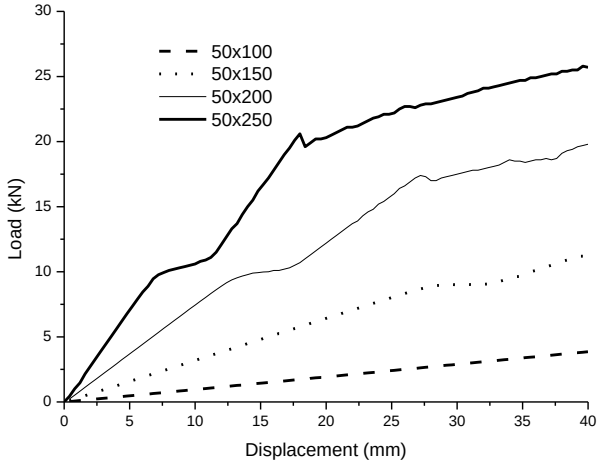

Figure 10. Parametric Study Influences of Ratio of Height to Width (*d*/*b*) of Beam Cross-section

Conclusions

This study develops nonlinear finite element analysis of LVL beam using MSC Marc/Mentat where the LVL Sengon layers is assumed as perfectly-plastic material. The glue contact is applied to Sengon beam elements, while touching contact is applied between LVL Sengon beams and steel supports as well as load plates. This proposed FEA model improves numerical model previously developed by co-author of this paper. The results of this proposed FEA model show that the load-deflection results have a similar trend with the experimental results including in the nonlinear response. The load at the maximum displacement of 38.59 mm is less than 10% difference where the FEA is about 25.7 kN and experimental result is about 27.88 kN, respectively. The failure mode of proposed FEA at maximum displacement 38.59 mm shows the same phenomenon as that of the experimental results including the local damage below the loading steel. The local damage according to the failure index of FEA results show the same location as that of experimental results. The results of the FEA also show that the ultimate beam load with lateral support at both supports is increasing with the higher lateral support depth. The lateral support depth, however, has no effect on the stiffness of the beam. The ultimate beam load is increasing by the higher ratio of height-to-width (*d*/*b*) of beam cross-section.

References

1. Davis, S.J., Lewis, N.S., Shaner, M., Aggarwal, S., Arent, D., Azevedo, I.L., M.Benson, S., Bradley, T., Brouwer, J., and Chiang, Y., Net-zero Emissions Energy Systems, *Science* (80-.), 360(6396), 2018, p. eaas9793.
2. Gustavsson, L., Joelsson, A., and Sathre, R., Life Cycle Primary Energy Use and Carbon Emission of an Eight-storey Wood-framed Apartment Building, *Energy Building*, 42(2), 2010, pp. 230–242.
3. Guardigli, L., Monari, F., and Bragadin, M.A., Assessing Environmental Impact of Green Buildings Through LCA Methods: Acomparison between Reinforced Concrete and Wood Structures in the European Context, *Procedia Engineering*, 21, 2011, pp. 1199–1206.
4. Nässén, J., Hedenus, F., Karlsson, S., and Holmberg, J., Concrete vs. Wood in Buildings–An Energy System Approach, *Buildings Environment*, 51, 2012, pp. 361–369.
5. Asdrubali, F., Ferracuti, B., Lombardi, L., Guattari, C., Evangelisti, L., and Grazieschi, G. A Review of Structural, Thermo-physical, Acoustical, and Environmental Properties of Wooden Materials for Building Applications, *Buildings Environment*, 114, 2017, pp. 307–332.
6. Sumarno A. and Ketikbuku, T.R., *Sengon & Jabon Kayu Super Cepat,* Penebar Swadaya Grup, 2012.
7. Awaludin, A., Firmanti, A., Theodarmo, H., and Astuti, D., Wood Frame Floor Model of LVL Paraserianthes Falcataria, *Procedia Engineering*, 171, 2017, pp. 113–120.
8. Awaludin, A. et al., Structural Performance of Prefabricated Timber-Concrete Composite Floor

Constructed Using Open Web Truss Joist Made of LVL Paraserianthes Falctaria, *Open Journal Civil Engineering*, 11(4), 2021, pp. 434–450.
9. Awaludin, A., Pribadi, A., and Satyarno, I., *Racking Resistance of Paraserianthes Falcataria Wooden Panel under Monotonic Load*, 2013.
10. Šorf, M. and Jandera, M., Lateral-torsional Buckling of Slender Cross-section Stainless Steel Beams, *Structures*, 28, 2020, pp. 1466–1478.
11. Awaludin A. and Wusqo, U., Evaluasi Perilaku Lentur Balok Tinggi LVL Sengon dengan Pengekang Lateral pada kedua Tumpuan, *MEDIA Komunikasi Teknik SIPIL*, 27(2), 2021, pp. 170–178.
12. Xiao, Q., Doudak, G., and Mohareb, M., *Lateral Torsional Buckling of Wood Beams: FEA-Modelling and Sensitivity Analysis*, WCTE, Quebec, 2014, pp. 1–8.
13. Hu, Y., Mohareb, M., and Doudak, G., Lateral Torsional Buckling of Wooden Beams with Midspan Lateral Bracing Offset from Section Midheight, *Journal Engineering Mechanics*, 143(11), 2017, p. 4017134.
14. Klasson, A., Crocetti, R., Björnsson, I., and Hansson, E.F., Design for Lateral Stability of Slender Timber Beams Considering Slip in the Lateral Bracing System, *Structures*, 16, 2018, pp. 157–163.
15. MSC, *MSC*, Softw. Corp. St. Ana, CA, 2012.
16. M.S.C., Marc, "Volume B: Element Library, MSC," Softw. Corp., 2012.
17. Awaludin, A., Irawati, I.S., and Shulhan, M.A., Two-dimensional Finite Element Analysis of the Flexural Resistance of LVL Sengon Non-prismatic beams, *Case Studies Construction Materials*, 10, 2019, p. e00225.
18. Siregar, U.J., Rachmi, A., Massijaya, M.Y., Ishibashi, N., and Ando, K., Economic Analysis of Sengon (Paraserianthes falcataria) Community Forest Plantation, a Fast Growing Species in East Java, Indonesia, *Policy and Economics*, 9(7), 2007, pp. 822–829.
19. Cazacu, O., New Yield Criteria for Isotropic and Textured Metallic Materials, *International Journal Solids Structure*, 139, 2018, pp. 200–210.
20. Moses, D.M. and Prion, H.G.L., Stress and Failure Analysis of Wood Composites: A New Model, *Composite Part B Eng*., 35(3), 2004, pp. 251–261.
21. Fueyo, J.G., Cabezas, J.A., Domínguez, M., Antón, N., and Villarino, A., Energy Distribution in Dowel-type Joints in Timber Structures when using Expansive Kits, *Forests*, 12(9), 2021, p. 1200.
22. Sun, X., He, M., and Li, Z., Novel Engineered Wood and Bamboo Composites for structural Applications: State-of-art of Manufacturing Technology and Mechanical Performance Evaluation, *Construction and Building Materials,* 249, 2020, p. 118751.
23. Guindos, P., Comparison of Different Failure Approaches in Knotty Wood, *Drew. Pr. Nauk. Doniesienia, Komun.,* 57, 2014.
24. Nali, P., and Carrera, E., A Numerical Assessment on Two-dimensional Failure Criteria for Composite Layered Structures, *Composite Part B Eng*., 43(2), 2012, pp. 280–289.
25. Sistaninia, M., Hudert, M., Humbert, L., and Weinand, Y., Experimental and Numerical Study on Structural Behavior of a Single Timber Textile Module, *Engineering Structuctures*, 46, 2013, pp. 557–568.
26. Barsanescu, P.D. and Comanici, A.M., Von Mises Hypothesis Revised, *Acta Mechanica*, 228(2), 2017, pp. 433–446.
27. Oka, G.M., Analisis Rasio antara Lebar dan Tinggi Balok terhadap Perilaku Lentur Kayu Kamper, *Smartek*, 7(1), 2009.